Available online at www.sciencedirect.com
ScienceDirect
Engineering Structures 30 (2008) 462–477
ENGINEERING STRUCTURES
www.elsevier.com/locate/engstruct

System identification of suspension bridge from ambient vibration response

Dionysius M. Siringoringo*, Yozo Fujino

Bridge & Structure Laboratory, Department of Civil Engineering, University of Tokyo, 7-3-1 Hongo, Bunkyo-ku, Tokyo 113-8656, Japan

Received 17 May 2006; received in revised form 5 March 2007; accepted 5 March 2007
Available online 25 May 2007

Abstract

The paper addresses and evaluates the application of system identification to a suspension bridge using ambient vibration response. To obtain dynamic characteristics of the bridge, two output-only time-domain system identification methods are employed namely, the Random Decrement Method combined with the Ibrahim Time Domain (ITD) method and the Natural Excitation Technique (NExT) combined with the Eigensystem Realization Algorithm (ERA). Accuracy and efficiency of both methods are investigated, and compared with the results from a Finite Element Model. The results of system identification demonstrate that using both methods, ambient vibration measurement can provide reliable information on dynamic characteristics of the bridge. The NExT-ERA technique, however, is more practical and efficient especially when applied to voluminous data from multi-channel measurement. The results from three days of measurements indicate the wind-velocity dependency of natural frequency and damping ratio particularly for low-order modes. The sources of these dependencies appear to be the effect of aerodynamic forces alongside the girder, and friction force from the bearing near the towers.
© 2007 Elsevier Ltd. All rights reserved.

Keywords: Ambient vibration measurement; System identification; Suspension bridge; Random decrement; Ibrahim Time Domain; Natural Excitation Technique; Eigensystem Realization Algorithm

1. Introduction

Performance of a suspension bridge under wind, seismic and other live loads depends upon its structural properties such as mass, stiffness and damping and their distribution. Although these properties can be modeled using sophisticated analytical models, the real behaviors of the bridge remain to be verified from a full-scale vibration test. The full-scale vibration test would facilitate identification of dynamic characteristics (e.g. natural frequency, damping ratio and mode shape), whose quantities serve as the basis for validating and/or updating analytical models of the structure, as well as providing the actual structural properties and boundary conditions. Furthermore, frequent measurements and analysis of these characteristics will facilitate the evaluation of structural safety and health monitoring.

There are two most common techniques for vibration test of a bridge, namely, the measured-input test and the ambient vibration test. In the measured-input, tests the structure is excited by artificial means using large inertial shakers or drop weights. Measured input excitation is usually applied at a single location where the force input to the structure can be monitored. The tests with measured inputs are usually conducted on small- or moderate-span bridges. The results are generally sufficient for modal identification since the inputs can be well defined and the excitations can be optimized to the response of vibration modes of interest. However, the test features that require extensive instrumentations and disruption of traffic have made frequent tests less favorable. Furthermore, in the case of large and flexible bridges (such as cable-stayed and suspension bridges), where the natural frequencies of the predominant modes are closely spaced within the frequency range 0–1 Hz, the controlled use of specific exciters to obtain significant levels of response is often difficult and costly. In such cases, ambient vibration becomes the only practical means of exciting the structure. This type of test makes use of ambient environment effects such as wind, traffic load, and environmental load as excitation force.

Ambient vibration tests have been successfully applied to a number of large bridges such as the Vincent Thomas suspension bridge [1], the Golden Gate suspension bridge [2],

* Corresponding author. Tel.: +81 03 5842 6097; fax: +81 03 5842 27454.
E-mail address: dion@bridge.t.u-tokyo.ac.jp (D.M. Siringoringo).

0141-0296/$ - see front matter © 2007 Elsevier Ltd. All rights reserved.
doi:10.1016/j.engstruct.2007.03.004



Fig. 1. View of the Hakucho Suspension Bridge.

Commodore Barry Bridge [3], Humber suspension bridge [4] and Vasco da Gama cable-stayed bridge [5] to mention a few. The results provided reliable and accurate estimates of natural frequencies and mode shapes, despite relatively small amplitudes of response.

The paper presents a schematic study on data analysis and evaluation of system identification procedures for modal parameter identification of a suspension bridge based on ambient vibration measurement. Since the measured responses are only ambient responses, system identifications that rely upon output measurements are adopted. This type of system identification is commonly called the *output-only system identification* or *operational modal analysis* [6]. Two operational modal analysis methods are applied and evaluated in this study, namely the Random Decrement combined with the Ibrahim Time Domain (RD-ITD) [7,8], and the Natural Excitation Technique (NExT) [9] paired with the Eigensystem Realization Algorithm (NExT-ERA) [10]. The study focuses mainly on two issues: (1) study of modal parameter identification using ambient response by the two operational modal analysis methods mentioned above, (2) evaluation of the sensitivity of modal parameters with respect to the ambient condition during the test, in this case wind velocity. Finally findings and conclusions of the study are summarized at the end.

2. The Hakucho Suspension Bridge

The bridge studied in this research is Hakucho Suspension Bridge (Fig. 1), which located at the entrance of Muroran Gulf in Hokkaido Prefecture, in the northern part of Japan. The bridge is built in a windy, seismically active and cold area. In fact it is the first Japanese suspension bridge constructed in such a snowy area so that a new technique to handle the snow accumulation was adopted during construction. The bridge has the total length of 1380 m, which consists of 720 m center span and two symmetric side spans of 330 m (Fig. 2). Both side spans and the center span are simply supported at the towers. The girder is made of a streamlined steel box girder with a width of 23 m and a maximum web height of 2.5 m. The bridge pylons are made of steel box girder and connected by welding. Both towers are 131 m high and 21 m wide. The construction of the bridge was started in 1985 and ended in 1998. It is finally opened to the public on June 13, 1998. After the construction completion, series of dynamic tests were performed, including ambient vibration test.

3. Ambient data analysis and methodologies

System identification using output-only ambient response was originally started with frequency analysis. In the frequency domain, the relationship between unknown inputs $u(t)$ measured at m locations and outputs $y(t)$ recorded at q locations is expressed as [11]:

$$\mathbf{G_{yy}}(f) = \mathbf{H}^{*}(f)\mathbf{G_{uu}}(f)\mathbf{H}(f)^{\mathrm{T}} \tag{1}$$

where $G_{xx}(f) = 2\int_{-\infty}^{\infty} R_{xx}(\tau)\mathrm{e}^{-\mathrm{i}2\pi f\tau}\mathrm{d}\tau$ denotes the power spectra density (PSD) of the input responses (for subscript **uu**) and of the output (for subscript **yy**) responses, and with $R_{xx}(\tau)$ denoting an even function of the cross-correlation of the signal $x(t)$. In the case of a multi-input and multi-output (MIMO) system, $\mathbf{G_{uu}}$ is a $m \times m$ PSD matrix, and $\mathbf{G_{yy}}$ is a $q \times q$ PSD matrix of the responses. $\mathbf{H}(f)$ is a $q \times m$ frequency response function (FRF) matrix, with superscript $(*)$ and T representing the complex conjugate and matrix transpose, respectively. Therefore, using N modes, $\mathbf{H}(f)$ becomes

$$\mathbf{H}(f) = \sum_{k=1}^{N}\left[\frac{Q_k\phi_k}{\mathbf{i}f-\lambda_k} + \frac{Q_k^{*}\phi_k^{*}}{\mathbf{i}f-\lambda_k^{*}}\right]. \tag{2}$$

In the equation above, λ_k denotes the kth pole (which occurs in complex conjugate pairs) of the system that associates with natural frequency and damping ratio. The matrices Q_k and ϕ_k represent the quantities of modal participation factor and mode shape vector respectively. For a linear system, when the input is assumed to be a stationary random process, the PSD of the input matrix $\mathbf{G_{uu}}(f)$ will yield a constant matrix (i.e. $(\mathbf{G_{uu}}(f) = \alpha)$). Therefore the PSD of output signal can be related to the cross spectra density of the random response as:

$$\mathbf{G_{yy}}(f) = |\mathbf{H}(f)|^2\alpha. \tag{3}$$

Hence, by computing the cross spectra matrix of output responses using the Fourier transform of the cross correlation functions, the poles that appear as peaks in the spectra density can be retrieved, since the PSD equation is now a linear product of the FRF and scalar α.

The method of selecting peaks in frequency domain of spectra density is generally called the peak-picking (PP) method, and has been used extensively in classical modal testing using ambient vibration. Several techniques were later developed to facilitate an automatic 'picking' procedure, such as frequency decomposition using singular value decomposition of PSD [12]. However, in practice the classical identification techniques that use spectra analysis give reasonable estimates of natural frequencies and mode shapes only if the modes are well separated. In the case of a large and flexible structure such as a suspension bridge, the modes are closely packed in frequency. This makes the estimation of natural frequency difficult, since almost all peaks are not well-separated. Moreover, the estimation of damping ratio using the half-power spectra bandwidth becomes more complicated since the widths of the spectra peaks are not very clear and often overlapped.

In time domain, two main approaches have been developed. The first methodology is called the Covariance-Driven Time-

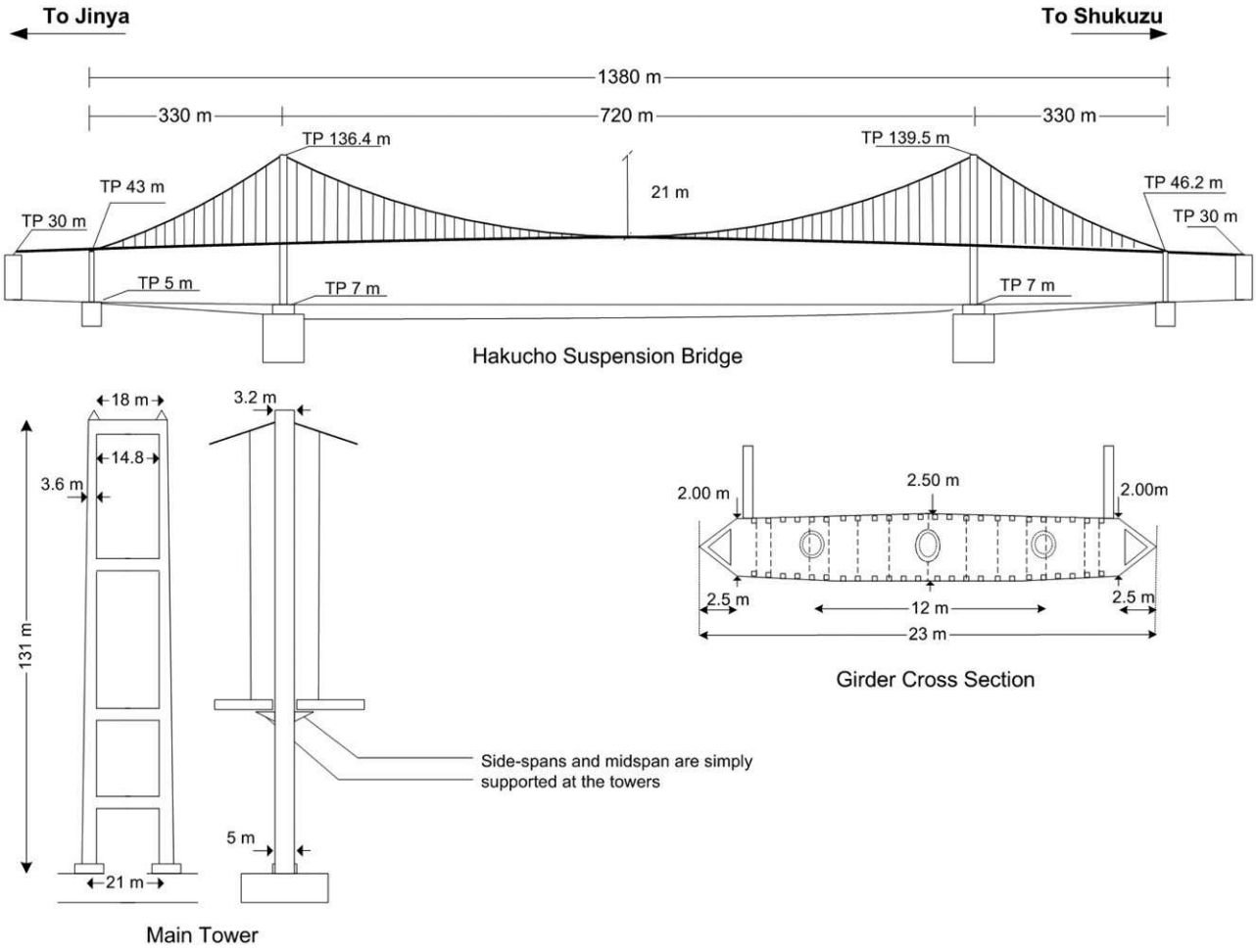


Fig. 2. Bridge layouts and dimensions.

Domain (CDTD), in which the modal identification is performed in two steps; the first step is to obtain the impulse response function or output covariance of a system excited by white noise; and the second step is modal extraction using modal identification techniques that can work with the free vibration response. There are two categories of such methods developed, one is the Instrumental Variable method (IV) and the other is the Covariance-Driven Stochastic Subspace Identification (SSI-COV) [6,13].

The IV method basically corresponds to the Polyreference Time Domain (PTD) [14] after substituting the impulse responses by the output covariance. Among the few methods that belong to this group are the Least Square Complex Exponential (LSCE) [15] and the Ibrahim Time Domain (ITD) [8]. Both are widely used for modal identification. The SSI-COV method can be considered as an enhancement of the IV method. The SSI-COV method deals with the stochastic realization problem, in which a deterministic realization is sought by using covariance of output data and singular value decomposition (SVD) technique. The Eigensystem Realization Algorithm (ERA) is one widely used method that belongs to the SSI-COV category.

The second type of time-domain methodology extracts modal properties in one step by directly using the measurement data, hence the term Data-Driven Time-Domain (DDTD). Unlike the CDTD, the data-driven method avoids computation of covariance between outputs. Two most commonly used methods that belong to this group are the Stochastic Subspace Identification (SSI-Data) [16] and the ARMA-based Prediction Error Model (PEM) [17].

Both CDTD and DDTD methods generally perform well concerning the modal parameters estimations (see for instance comparison work by [6]). The main difference between the two is the computational load. The DDTD methods that require QR factorization are typically slower than the CDTD. In the CDTD method, effects of randomness and transients can be eliminated by means of correlation between outputs, while in the DDTD method, this feature is not explicitly defined. Furthermore, the DDTD method may result in modal properties that have no physical meaning due to the presence of noise in responses or due to small non-linearity of the structures. Therefore a post-processing interpretation of the outcome becomes very important.

To avoid drawbacks in frequency domain identification and the time domain DDTD method, in this research, the time domain CDTD method is adopted. Furthermore, in order to compare performance between the IV-based and the SSI-COV-based method, two techniques namely Ibrahim Time Domain (ITD) and the ERA were adopted. Since both ITD and ERA rely on initial information from impulse response function (IRF)

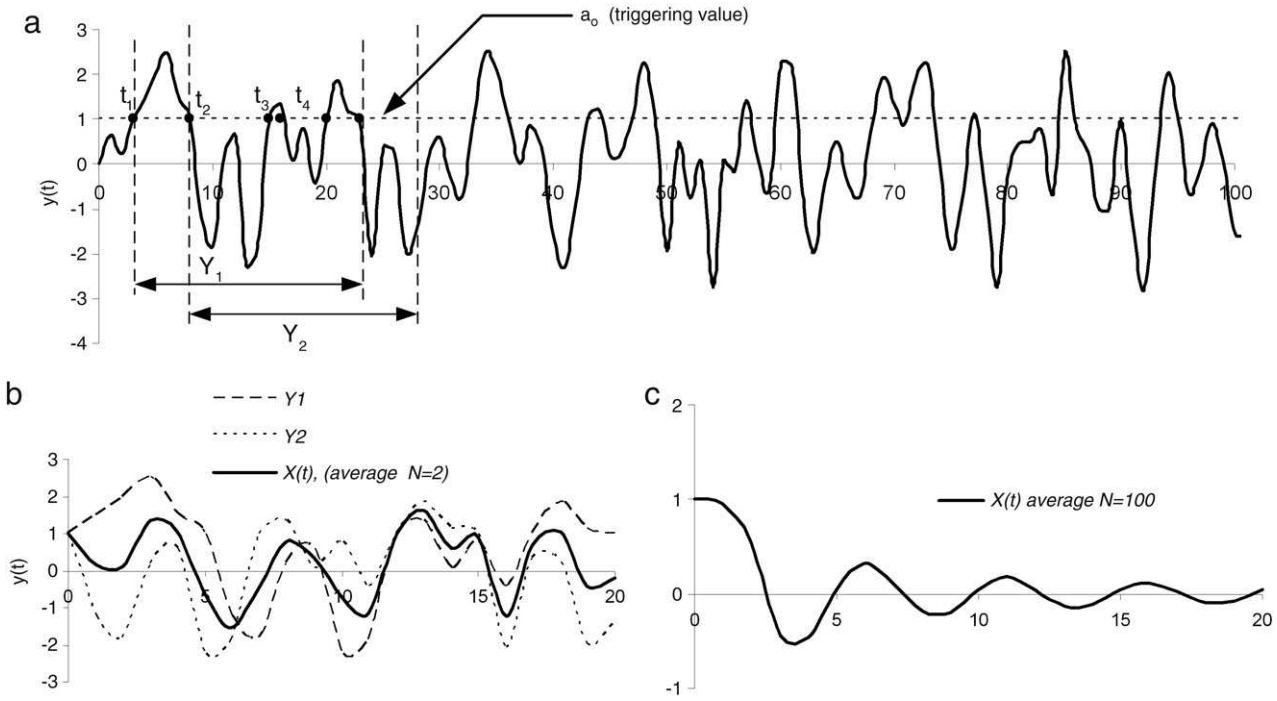


Fig. 3. Schematic figure of Random Decrement technique. (a) Random response divided into several equal-length time frames using the triggering value a_0. (b) Free decay response synthesized using $N = 2$ frames of random response. (c) Free decay response synthesized using $N = 100$ frames of random response.

or output covariance, two techniques that are commonly used for deriving the IRF are adopted. These techniques are the Random Decrement (RD) for ITD and the Natural Excitation Technique (NExT) for ERA. RD and ITD tehniques have been frequently utilized for modal identification of structure given the advantage of their straightforward adaptation to the multi output system with simultaneous measurement [7,8,18–20]. Apart from the application with ITD, the RD technique is also commonly used to estimate damping of structures [21]. Compared to RD-ITD, NExT-ERA is a relatively new method. Nevertheless, it also has been successfully applied to structural identification based on ambient measurement [22,23]. In both references, however, the method was applied to relatively smaller laboratorial scale objects. An application to a large and real structure is examined in this study. For the sake of completeness the methods are discussed briefly in the following sections.

3.1. Random Decrement technique

The Random Decrement (RD) technique [7] is based on assumption that dynamic response of a structure under ambient excitation at a time instant t_0 to $t + t_0$ can be divided into three components:

1. Deterministic part of step response due to initial displacement at time $t = t_0$.
2. Deterministic part of impulse response function due to initial velocity v_0.
3. Random part due to random excitation applied to the structure in interval time t_0 to $t + t_0$.

The RD procedure starts by selecting an appropriate initial value of the response, from which the equally-spaced segments of $\langle t_0, t + t_0 \rangle$ time histories are extracted. These segments are then averaged in order to even out the random parts and to retain only the deterministic part of the response (as shown in Fig. 3).

In Eq. (4), it is shown that if $y(t)$ is a random time history sampled from t_i to $t_i + \tau$, then the free vibration (free-decay) response $x(\tau)$ is obtained after averaging N sets of time histories with equal time length τ. To avoid averaging out the deterministic part, the segmented time history can be taken starting always with the following conditions: (1) constant level, which will give the free-decay step response, (2) positive slope and zero level, which will produce a free-decay positive impulse response, (3) negative slope and zero level, which will give the free-decay negative impulse response.

$$x(\tau) = \frac{1}{N} \sum_{i=1}^{N} y(t_i + \tau). \tag{4}$$

Vandiver et al. [24] reveal that if a stationary Gaussian random process excites a linear system, then the RD-generated random signature of that response will have similar characteristics as a free vibration response of that linear system under a specified initial condition.

3.2. Ibrahim Time Domain (ITD)

In conjunction with Random Decrement, Ibrahim Time Domain (ITD) is employed. In this method, natural frequency, damping ratio, and mode shape are estimated directly from the free-decay response of random decrements. Consider a matrix equation of free-decay responses $\mathbf{X}$ of an N degree-of-freedom system measured at q response locations during L time instants:

$$\mathbf{X} = \mathbf{\Phi\Lambda} \tag{5}$$

where:

$$\mathbf{X} = \begin{bmatrix} x_1(t_1) & x_1(t_2) & \cdots & x_1(t_L) \\ x_2(t_1) & x_2(t_2) & & x_2(t_L) \\ \vdots & & \ddots & \vdots \\ x_q(t_1) & x_q(t_2) & \cdots & x_q(t_L) \end{bmatrix},$$

$$\mathbf{\Phi} = \begin{bmatrix} \phi_{11} & \phi_{12} & \cdots & \phi_{12N} \\ \phi_{21} & \phi_{22} & & \phi_{22N} \\ \vdots & & \ddots & \vdots \\ \phi_{q1} & \phi_{q2} & \cdots & \phi_{q2N} \end{bmatrix},$$

$$\text{and} \quad \mathbf{\Lambda} = \begin{bmatrix} e^{\lambda_1 t_1} & e^{\lambda_1 t_2} & \cdots & e^{\lambda_1 t_L} \\ e^{\lambda_2 t_1} & e^{\lambda_2 t_2} & & e^{\lambda_2 t_L} \\ \vdots & & \ddots & \vdots \\ e^{\lambda_{2N} t_1} & e^{\lambda_{2N} t_2} & \cdots & e^{\lambda_{2N} t_L} \end{bmatrix}.$$

In Eq. (5), it is reasonable to assume that $2N \leq q \leq L$. Matrix $\mathbf{\Phi}$ is the eigenvector matrix whose element ϕ_{ij} denotes the jth vector component measured at location i. Matrix $\mathbf{\Lambda}$ is the eigenvalue matrix whose element $e^{\lambda_j t_k}$ is a product of the jth eigenvalue and the kth time step.

Now, consider the second set of L data, measured at the same q locations, but shifted one time interval Δt with respect to the first time sampling. The new equation now yields:

$$\hat{\mathbf{X}} = \hat{\mathbf{\Phi}}\mathbf{\Lambda}. \tag{6}$$

In Eq. (6), $\hat{\mathbf{X}}$ is now the matrix of free-decay response with the element of $\hat{x}_i(t_k) = x_i(t_k + \Delta t)$, and matrix $\hat{\mathbf{\Phi}}$ elements become $\hat{\phi}_{ij} = \phi_{ij} e^{\lambda_j \Delta t}$. Following the relationship in Eqs. (5) and (6), one can define a system matrix $\mathbf{A}$ with the size of $q \times q$ that connects the initial eigenvector matrix with the shifted one as:

$$\mathbf{A}\mathbf{\Phi} = \hat{\mathbf{\Phi}}. \tag{7}$$

After some matrix manipulations, and by substituting $\mathbf{\Phi}$ and $\hat{\mathbf{\Phi}}$ in Eq. (7) with Eqs. (5) and (6) respectively, the following equation is obtained:

$$\mathbf{A}\mathbf{X} = \hat{\mathbf{X}}. \tag{8}$$

Eq. (8) states that the system matrix $\mathbf{A}$ can be identified via pseudo-inverse techniques by knowing only the original free-decay and its shifted response matrix. Furthermore, using the definition of $\hat{\mathbf{\Phi}}$ in Eq. (6), Eq. (7) can be rewritten as:

$$[\mathbf{A} - e^{\lambda_j \Delta t}\mathbf{I}]\phi_j = \{0\}. \tag{9}$$

Eq. (9) is a standard eigenvalue problem, involving each eigenvector ϕ_j. Solving Eq. (9) will yield the eigenvector that corresponds to the eigenvalue of system matrix $\mathbf{A}$. The derivation given here is necessarily simplistic; more details on the identification procedure are given in [8].

3.3. Natural Excitation Technique (NExT)

The basic principle of NExT states that the cross-correlation function between two responses made on an ambient-excited structure has the same analytical form as the impulse response function (or the free vibration response) of the structure. In order to understand this concept, a brief explanation will be provided; readers are advised to refer to the work by Farrar and James III [9] for full derivation of the method.

Let the response $x_i^k(t)$ at location i caused by an input force $f_k(t)$ at location k be defined as:

$$x_i^k(t) = \sum_{r=1}^{N} \phi_i^r \phi_k^r \int_{-\infty}^{t} f_k(\tau) g^r(t-\tau) \mathrm{d}\tau \tag{10}$$

with $g^r(t) = (1/m^r \omega_d^r) e^{-\zeta^r \omega_n^r t} \sin(\omega_d^r t)$ represents the impulse response function associated with mode r. Vector ϕ^r and ω_d^r are the mode shape vector and damped natural frequency of mode r, respectively, with N denoting the number of modes. When $f_k(t)$ is a Dirac delta function, Eq. (10) yields

$$x_i^k(t) = \sum_{r=1}^{N} \frac{\phi_i^r \phi_k^r}{m^r \omega_d^r} e^{-\zeta^r \omega_n^r t} \sin(\omega_d^r t). \tag{11}$$

Now, on the basis of assumption that $f_k(t)$ is a random white noise function and by employing the definition of cross-correlation between responses at point i and j, excited by a force at point k:

$$\mathbf{R}_{ij}^k(T) = E\{x_i^k(t+T) x_j^k(t)\}, \tag{12}$$

the cross-correlation $\mathbf{R}_{ij}^k(T)$ between two ambient responses can be defined as:

$$\mathbf{R}_{ij}^k(T) = \sum_{r=1}^{N}\sum_{s=1}^{N} \phi_i^r \phi_k^r \phi_j^s \phi_k^s \int_{-\infty}^{t}\int_{-\infty}^{t+T} g^r(t+T-\sigma) \times g^s(t-\sigma) E\{f_k(\sigma) f_k(\tau)\} \mathrm{d}\sigma \mathrm{d}\tau. \tag{13}$$

Afterwards, by using the definition of autocorrelation function:

$$E\{f_k(\sigma) f_k(\tau)\} = \alpha_k \delta(\tau - \sigma) \tag{14}$$

where $\delta(t)$ denotes the Dirac delta function, the last part of the right-hand side of Eq. (13) can be simplified, and the equation becomes:

$$\mathbf{R}_{ij}^k(T) = \sum_{r=1}^{N}\sum_{s=1}^{N} \alpha_k \phi_i^r \phi_k^r \phi_j^s \phi_k^s \int_0^{\infty} g^r(\lambda + T) g^s(\lambda) \mathrm{d}\lambda. \tag{15}$$

The variable of integration in Eq. (15) is changed to $\lambda = t - \tau$. In Ref. [9] it is shown that the cross-correlation functions between two measurement responses obtained from an unknown white noise excitation as expressed in Eq. (15) will have the form of decaying sinusoids scaled by a factor. Therefore, these decaying sinusoids have the same characteristics as the system's impulse response function. When implemented in practice the cross-power spectra were initially derived and then transformed to time domain using the inverse Fourier transform to obtain the cross-correlation function.

3.4. Eigensystem Realization Algorithm (ERA)

The ERA [10] is a time-domain system identification based on the evolution of the Ho–Kalman [25] method, which

introduces the concept of minimum realization. The minimum realization method identifies a system model with the smallest state dimension that holds an equivalent relationship of input-output as in the real system. The basic principal of ERA involves identification of system matrix **A** from free-vibration responses. At first, let consider an equation of motion of a discrete structural system under acting vector force $\mathbf{f}(t)$ be expressed in the first-order form of a state-space equation:

$$\dot{\mathbf{z}}(t) = \mathbf{A}\mathbf{z}(t) + \mathbf{B}\mathbf{f}(t) \tag{16}$$

where the matrices are defined as:

$$\mathbf{A} = \begin{bmatrix} -\mathbf{M}^{-1}\mathbf{K} & -\mathbf{M}^{-1}\mathbf{C} \\ \mathbf{I} & \mathbf{0} \end{bmatrix}, \quad \mathbf{z}(t) = \begin{bmatrix} \dot{\mathbf{x}}(t) \\ \mathbf{x}(t) \end{bmatrix} \quad \text{and} \quad \mathbf{B} = \begin{bmatrix} \mathbf{M}^{-1} \\ \mathbf{0} \end{bmatrix}. \tag{17}$$

The frequency (ω) and damping ratio (ζ) of the mass **M**, damping **C** and stiffness **K** system appear as conjugate pairs of the eigenvalues of matrix **A**:

$$\lambda_{\mathbf{A}} = -\zeta\omega \pm \mathrm{i}\omega\sqrt{1-\zeta^2}. \tag{18}$$

In the case of free vibration, the eigenvectors of **A** become the eigenvectors of the equation of motion (Eq. (16)). Therefore, once the matrix **A** can be realized from measurement, modal parameters of the system can be extracted.

ERA identifies a candidate of matrix **A** from IRFs of a multi-mode system. The IRF can be shown to be equivalent and contain the same information, and accordingly can be derived using following methods:

1. Measurement of free-decay in time domain directly.
2. Inverse Fast-Fourier Transform (FFT) of the frequency response functions.
3. Cross-correlation functions of random response.
4. Inverse FFT of the cross-spectral densities of random responses.

In this study to obtain the IRFs, initially the cross-power spectra between random responses measured at the reference channels and the other random responses from multi channels located at various positions on the bridge were computed. Afterwards these spectra were transformed back into time-domain using the inverse Fourier transform to obtain the cross-correlation functions.

Information from IRF at the discrete kth time sample, defined as $\mathbf{Y}_k$, is stacked to form a matrix known as the Hankel matrix 'at time 0':

$$\mathbf{H}(\mathbf{0}) = \begin{bmatrix} \mathbf{Y_0} & \mathbf{Y_1} & \cdots & \mathbf{Y_r} \\ \mathbf{Y_1} & \mathbf{Y_2} & & \mathbf{Y_{r+1}} \\ \vdots & & \ddots & \vdots \\ \mathbf{Y_s} & \mathbf{Y_{s+1}} & \cdots & \mathbf{Y_{r+s+2}} \end{bmatrix}. \tag{19}$$

This discrete time sample $\mathbf{Y}_k$ is also known as the Markov parameter. As the Markov parameters contain information from IRFs, which represent vibration characteristics of the structure, the modal parameters can therefore be identified from the Hankel matrix. The scalar r and s in $\mathbf{H}(\mathbf{0})$ are parameters that define the number of samples used, and they require a certain balance to cover the long frequency components of IRFs. As more rows and columns added to the $\mathbf{H}(\mathbf{0})$, the rank increases until it covers all vibration modes that contribute to the responses.

Afterwards, the minimum rank of $\mathbf{H}(\mathbf{0})$ is computed and a state matrix **A** is realized from it. To select the system order, the singular value decomposition (SVD) of the Hankel matrix is performed:

$$\mathbf{P}\mathbf{D}\mathbf{Q}^{\mathbf{T}} = SVD[\mathbf{H}(\mathbf{0})]. \tag{20}$$

The rank of the Hankel matrix is selected by retaining the N largest singular values. The SVD procedure works in such a way that the larger singular values associated with the real modes come first in order, while the smaller singular values associated with computational or fictitious modes come last in order. Therefore, the state matrix **A** can be identified by retaining the first N sub-vectors as follows:

$$\mathbf{A} = \mathbf{D}_{\mathbf{N}}^{-\mathbf{1/2}}\mathbf{P}_{\mathbf{N}}^{\mathbf{T}}\mathbf{H}(\mathbf{1})\mathbf{Q}_{\mathbf{N}}\mathbf{D}_{\mathbf{N}}^{-\mathbf{1/2}}. \tag{21}$$

The eigenvalues that contain natural frequencies and damping ratios are identified by solving the eigenvalue problem of matrix **A**. Likewise, the eigenvectors of **A** become the eigenvectors of the system.

The presence of inevitable measurement noise introduces uncertainty about the rank of the generalized Hankel matrix as well as uncertainty of the modal parameters. In order to distinguish the real modes from computational, fictitious or noise-generated modes, ERA introduces indicators such as the Extended Modal Assurance Criteria (EMAC) of observability and controllability matrix [26]. The EMAC indicator measures degree of coherence between an identified mode and its ideal counterpart, projected on a time frame at the later moment. The basic principle of EMAC states that if a mode is indeed a genuine mode, then it can be identified at any time frame during the measured time histories. On the other hand, if a mode is a fictitious or computational mode, then it only appears arbitrarily at certain time frames. The real modes usually result in EMAC values close to 100%, while the computational or noise-generated modes give less than 70% coherency. EMAC indicators measure modes coherency in both observability and controllability matrices, thus provide tools to observe how consistent a mode shape vector is throughout a time history.

4. Application to ambient response of the Hakucho Bridge

4.1. Ambient response measurement

To measure dynamic responses of the Hakucho Suspension Bridge, densely distributed accelerometers were placed at various locations. On the girder, twenty-one accelerometers were installed with the spacing of 30 m on the main span and of 55 m on the side span near the Jinya approach. Of these 21 accelerometers, 17 were placed on the centerline of the bridge deck, while the other four were mounted on both sides of the

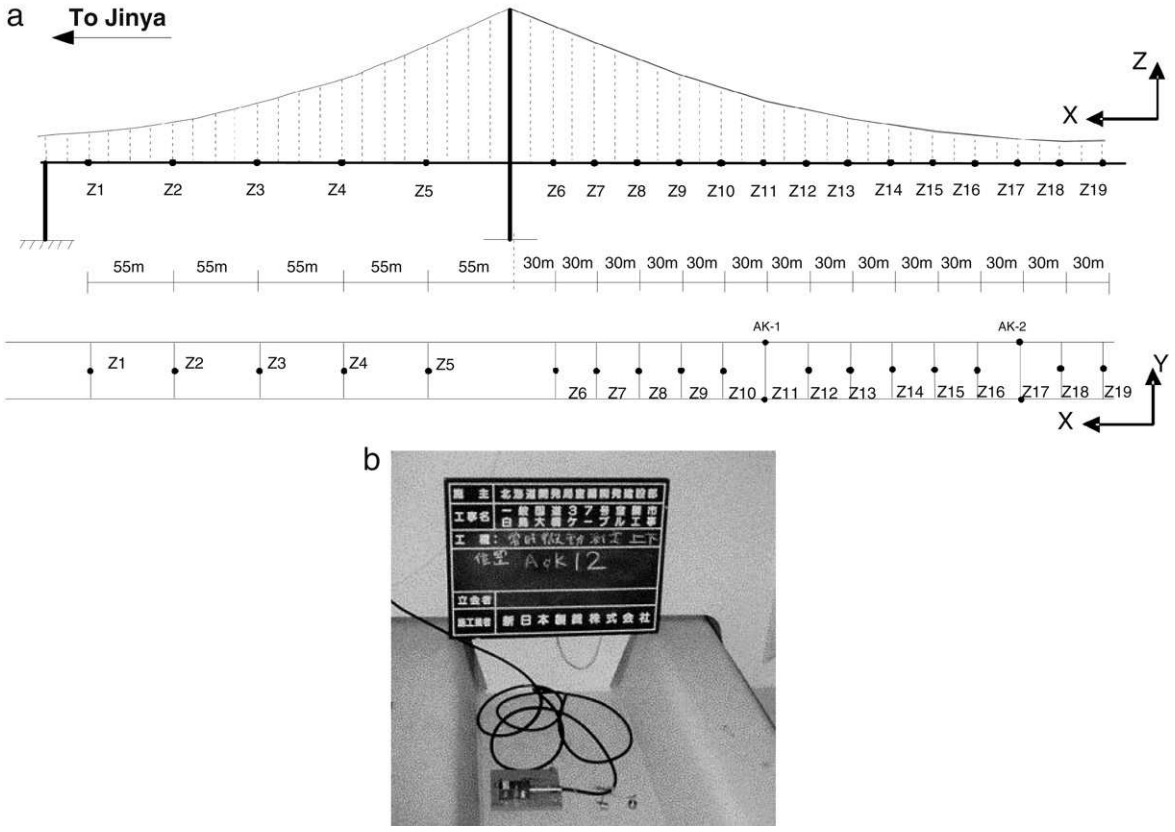


Fig. 4. (a) Sensor positions and measuring direction, (b) Accelerometer placed on the girder at Z12 position.

middle span to cover the torsional motion of the bridge. Fig. 4 illustrates the sensor configuration, measuring direction and typical accelerometer used in measurement. In order to measure wind velocity an anemometer was installed at the center of the span of the deck. Since this bridge is located at the port entrance, wind orthogonal to the bridge is relatively strong.

The measurement was started on June 4, 1998 and ended on June 12, 1998. During this period, data were observed and collected every 15 min. The continuous ambient measurement in this study has three important features compared to the previous ambient tests conducted on the long span bridges in Japan: (1) the total time of measurement is more than 200 h, which allows us to eliminate statistically the influence of randomness of other forces, (2) the number of measurement stations is relatively dense (21 stations), this provides more comprehensive spatial information that would lead to good results especially for the mode shape estimation, (3) all measurement stations work simultaneously, thus no time synchronization is required.

4.2. Results of the RD-ITD identification

Random responses from 21 measurement channels shown in Fig. 4 were analyzed using the RD method to synthesize free vibration responses. Eq. (4) shows that before implementing the RD, one needs to determine the number of random samples $y(t)$ with equal initial value and time length. This number (N in Eq. (4)) depends upon triggering level, which in this case is the initial value of acceleration. The triggering value was determined by trial-and-error upon observing the resulted free-decay response. At the first attempt, the initial acceleration $a_0 = 0.285$ m/s^2 was selected. By applying this initial value, up to 50 time histories were obtained. This number was considered insufficient since the results still show larger random components and higher frequency noise (see for instance Fig. 5(b)).

The procedure was later repeated until ten thousands samples of random responses were included ($N = 10\,000$). This sampling number yields $a_0 = 0.09$ m/s^2. By observing the effect of the sample number to free vibration response, it was concluded that to create an acceptable free vibration response, at least 5000 random samples are required in the summation. This number of samples are obtained if the initial acceleration (a_0) is equal to 0.8 of the root-mean-square (*rms*) of the acceleration response. Fig. 5 shows typical ambient vertical acceleration of the girder measured at channel Z17 and its free vibration response obtained after applying the RD technique with several values of N. From this figure one can see the effectiveness of RD technique especially in reducing the random effect at higher frequency. The free vibration response obtained after applying RD is characterized by low frequency components that correspond to the natural frequencies of the bridge.

Since the matrix **A** in Eq. (9) is of order q, there will be q eigenvalues and eigenvectors. In the case where all identified modes are real modes, q is equal to $2N$. In practice, however, there will be several computational modes in addition to the

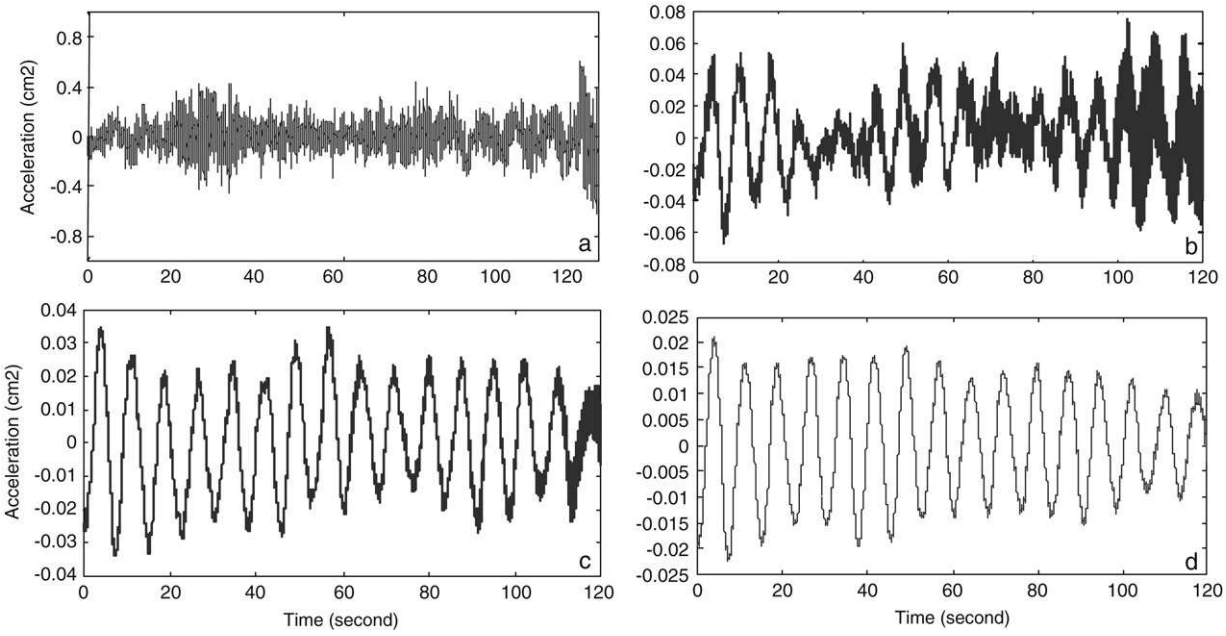


Fig. 5. Typical application of the Random Decrement technique to vertical response at station Z17 (half-span of the main girder) (a) original random response (b) free-vibration after 50 samples with $a_0 = 0.285$ cm/s^2, (c) free-vibration after 1000 samples with $a_0 = 0.18$ cm/s^2, (d) free-vibration after 10 000 samples with $a_0 = 0.09$ cm/s^2.

real modes thus leaving $q > 2N$. One way to differentiate computational modes from the real ones is by following the relationship: $\hat{\phi}_{ij} = \phi_{ij} e^{\lambda_j \Delta t}$.This relationship states that the consistency of an identified mode can be evaluated by repeatedly observing its presence in different time shifts. The modes that always appear in different time shifts can be considered as genuine modes, whereas those that do not appear frequently can be categorized merely as computational modes.

Direct implementation of ITD generated only the first three modes, namely the first and the second vertical symmetric bending modes, and the first anti-symmetric bending mode. It should be mentioned that during selection of random responses, wind velocity was kept constant. As a consequence, only very short periods of time histories, such as two or three-hour data, can be used directly in analysis. Owing to this restriction, the higher modes cannot be identified directly from ITD. Moreover, since the free-decay responses were dominated by low-frequency components, the higher frequency components cannot be identified directly.

In order to identify the higher modes, an additional approach that filters out the low frequency components using highpass filters was employed. The procedure begins by omitting the low frequency components from the free-decay responses. This was accomplished by transforming the free-decay responses into frequency domain and then passing them through a highpass Butterworth filter. Afterwards, the new filtered time-domain free vibration responses were generated using the inverse Fourier transform. These responses were utilized as the new input of ITD to generate the higher modes. The procedure was repeated several times until all modes were identified. Fig. 6 illustrates the outline of ITD and the filtering scheme. At the first attempt, by filtering out the frequency components smaller than 0.3 Hz, the first six modes were identified. These six modes

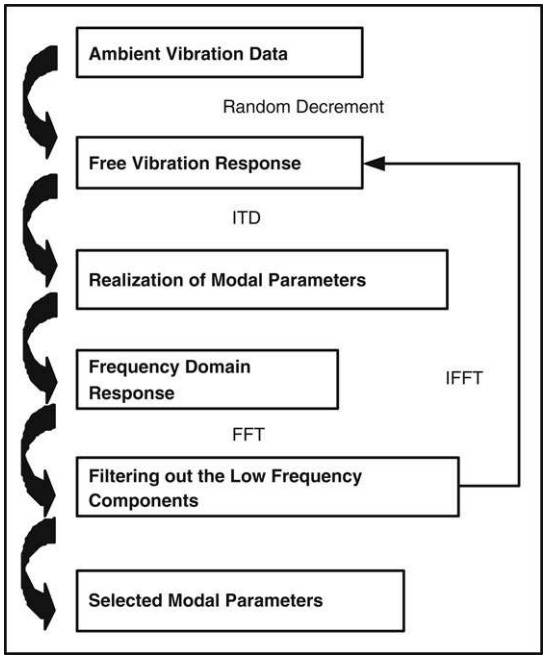


Fig. 6. Outline of the filtering method for ITD.

included three symmetric and three anti-symmetric bending modes. In the second attempt, the highpass filter of 1.0 Hz resulted in four new modes: two symmetric modes and two anti-symmetric modes. Filtering out all frequencies smaller than 1.5 Hz generated six new modes: three symmetric modes and three anti-symmetric modes. Finally all modes were identified after the fourth attempt using the threshold frequency of 2.0 Hz.

By employing this simple procedure, all vertical bending and torsional modes can finally be identified. Table 1 lists the natural frequencies and the type of all modes identified.

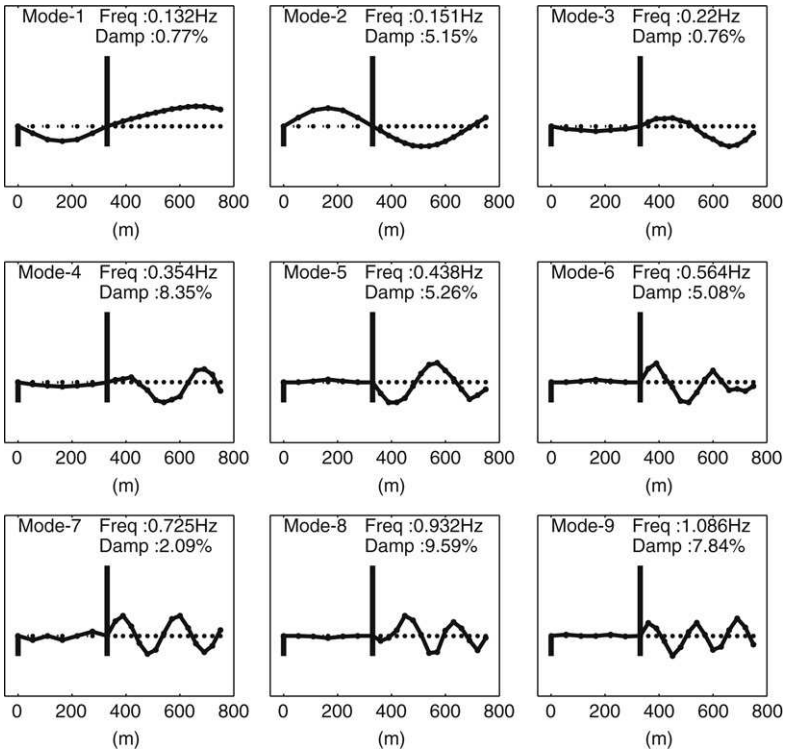


Fig. 7. Vertical bending mode shape identified using Random Decrement-ITD method.

Table 1
Identified modes from ambient vibration and comparison with FEM and forced vibration test

Mode number	Natural frequency (Hz)				Mode type (B = Bending,T = Torsion)
	Ambient vibration		FEM	Forced vibration test	
	NExT-ERA	RD-ITD			
1	0.132	0.132	0.126	0.129	1st symmetric (B)
2	0.153	0.151	0.151	0.149	1st anti symmetric (B)
3	0.220	0.220	0.220	0.218	2nd symmetric (B)
4	0.367	0.354	0.322	0.317	2nd anti symmetric (B)
5	0.439	0.438	0.439	0.435	3rd symmetric (B)
6	0.500	0.496	0.472	0.478	1st symmetric (T)
7	0.574	0.564	0.570	0.568	3rd anti symmetric (B)
8	0.733	0.725	0.722	0.719	4th symmetric (B)
9	0.792	0.791	0.778	0.772	1st anti symmetric (T)
10	0.965	0.932	0.900	0.906	4th anti symmetric (B)
11	1.058	1.086	1.079	N/A	5th symmetric (B)
12	1.190	1.182	1.160	1.164	2nd symmetric (T)
13	1.149	1.178	1.295	N/A	5th anti symmetric (B)
14	1.528	1.525	1.523	N/A	6th symmetric (B)
15	1.566	1.568	1.530	1.502	2nd anti symmetric (T)
16	1.923	1.909	1.766	N/A	6th anti symmetric (B)
17	1.930	1.958	1.860	1.866	3rd symmetric (T)
18	2.011	2.150	2.036	N/A	7th symmetric (B)
19	2.380	2.330	2.292	N/A	7th anti symmetric (B)
20	2.554	2.599	2.606	N/A	8th symmetric (B)
21	2.901	2.895	2.894	N/A	8th anti symmetric (B)
22	3.159	3.207	3.207	N/A	9th symmetric (B)
23	3.521	3.550	3.534	N/A	9th anti symmetric (B)
24	3.800	3.831	3.838	N/A	10th symmetric (B)

N/A: Not available.

Representative shapes of the vertical bending modes are shown in Fig. 7. The results are compared with the finite element model (FEM) and the forced vibration test (FVT). It can be observed that the identified frequencies are in good agreement with those identified from FVT and also with the finite element model. It should be mentioned that the results of frequency filtering in ITD depend on the knowledge of the range of frequency targets. Consequently, prior knowledge of natural

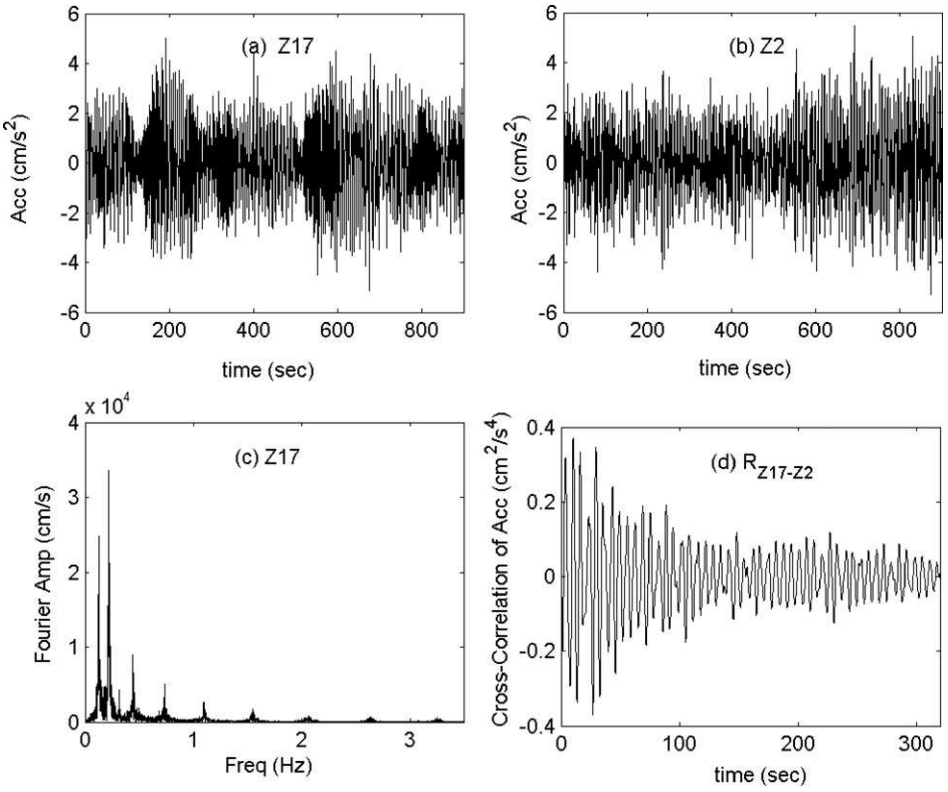


Fig. 8. (a) Typical ambient response of vertical acceleration at Z17 (b) typical ambient response of vertical acceleration at reference channel Z2, (c) Fourier spectrum of ambient response of vertical acceleration at Z17 (d) Free-vibration response derived using NExT (Correlation function between Z17 and Z2).

frequencies of the bridge obtained from analytical models can be very helpful.

4.3. Results of NExT-ERA identification

As mentioned in the previous section, the IRFs for NExT-ERA method are derived from inverse Fourier transform of the cross-power spectra between responses at designated reference channels and the other measurement responses located at the various positions on the bridge. Therefore, the first step in implementing NExT is to select the reference channels. For this purpose several candidates were evaluated. At first attempt, channels number Z18 and Z19 were chosen as references. The two channels were selected so that the remaining channels (Z1 to Z17) would cover the half span of the bridge. It should be mentioned that channel AK-1 and AK-2 were excluded in identification of vertical bending modes. They were later included during the identification of torsional modes.

Selecting channels Z18 and Z19 as the reference led to the size of Markov parameter (i.e. $\mathbf{Y}_k$ in Eq. (19)) of 17×2. After evaluating modal parameters resulted from this selection, it was found that only the first five low-order modes were identified. Three size of Hankel matrix were initially utilized, namely, $s = r = 100, 200$, and 400. In the second attempt, five channels from the side span (Z1 to Z5) were selected as the reference, and the other fourteen channels (Z6 to Z19) were used as output responses. This selection led to the Markov parameter with the size of 14×5. A total of 320 s impulse response functions were generated. Fig. 8 shows an example of impulse response function computed from channel Z17 and reference channel Z2. Again, three sizes of Hankel matrix were utilized namely, $s = r = 100$, 200, and 400. The optimal size of Hankel matrix was finally found to be $s = r = 400$, or about twenty seconds of impulse response functions at the rate of 20 samples per second. Using this selected reference channels and Hankel matrix size; the first 19 vertical bending modes were simultaneously identified. A singular value plot was used to facilitate the selection of singular value cutoff. Based on observation, a typical sudden drop in the plot appeared around 500, making this value as the singular value cutoff for modal truncation. The same procedure was employed to identify torsional modes. For this purpose, channels AK-1 and AK-2 were included in order to capture the torsional motion from the left and the right side of the girder. Again, five channels from the side span namely Z1 until Z5 were employed as reference channels, and the remaining sixteen channels were used as output responses. In ERA, the size of Hankel matrix $s = r = 400$ was used. This generated about twenty seconds of impulse response functions at the rate of 20 samples per second. The ERA identified five torsional vertical modes in addition to the 19 vertical bending modes.

The natural frequencies and type of mode of the vertical bending and torsional modes identified using NExT-ERA are reported in Table 1. The results from RD-ITD, Finite Element Model (FEM) and FVT are also listed for comparison. It can be seen that the identified natural frequencies from the two methods are in excellent agreement with each other and within reasonable agreement when compared to their FEM

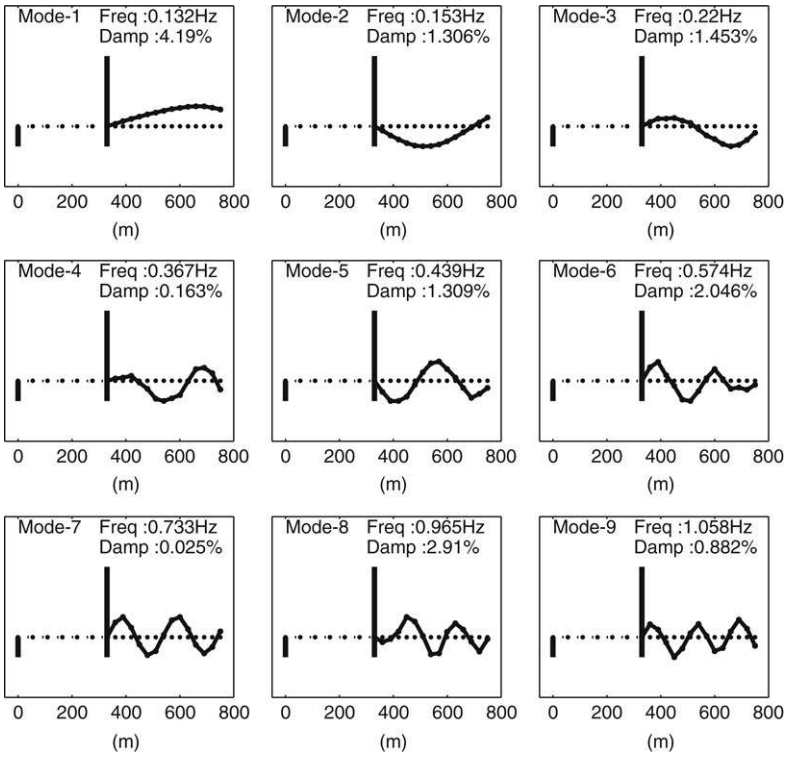


Fig. 9. Vertical bending mode shape identified using NExT-ERA method.

counterparts. Fig. 9 illustrates several representative modes identified using NExT-ERA. In this figure, the side-span's mode shapes do not appear, since the channels that correspond to the side-span were used as the reference channels.

It should be mentioned that several rectangular Hankel matrices with sizes of 120×150, 150×200 etc. were also used, but the results were not any better. We found the best results using a square Hankel matrix with $s = \gamma = 400$. When a singular value cutoff of 500 is utilized, theoretically there could be up to 250 modes realized. However, most of the modes were fictitious. To distinguish the real modes from the fictitious or computational ones, the following measures were taken. (1) By using the modal assurance criteria provided by ERA such as EMAC, the EMAC values of fictitious modes usually very small compared with the real ones, thus in the selection only modes with EMAC values larger than 80% were selected. (2) By judging from the shapes of the modes generated, in this case the mode shapes of a simply supported beam are used for comparison. (3) By judging from the generated modal damping ratio. Usually the fictitious modes have uncharacteristically large damping or even negative values. By employing these three measures, the fictitious modes could usually be sorted out.

5. Amplitude depedence of modal parameters

More than 200 h data from three-days of measurement were analyzed in this study. Efficient and effective system identification is obviously essential for processing such large amounts of data. As mentioned previously, identification of high order modes using RD-ITD is not as straightforward as identification using NExT-ERA. The RD-ITD requires filtering out the low frequency component to obtain higher frequency modes. This procedure is clearly time consuming and not deemed reasonable to be applied to 200 h of measurement data. Therefore, in the subsequent analysis, the NExT-ERA technique is employed. The implementation of NExT-ERA to 200 h of measurement data involves the following procedures.

(1) First, measurement data were divided into a number of frames consisting of 15 min ambient response each, with the field sampling frequency of 100 Hz.
(2) Based on these data, cross-power spectra between the reference channels (Z1 to Z5) and the output channels (Z6 to Z19) were computed.
(3) These spectra were transformed back into time-domain using the inverse Fourier transform to obtain the 320 s of cross-correlation functions.
(4) In ERA, the Hankel matrix of $s = r = 400$ was selected, which means twenty seconds of impulse response functions at the frequency sampling rate of 20 Hz was utilized.

5.1. An automatic procedure for modal selection

To facilitate an automatic identification, a post-processing procedure that follows the ERA realization is added. In this scheme, the real modes are selected from a pool of generated modes, by employing the sequential mode-selector procedures below:

1. Remove all modes with EMAC values less than 80%, or having negative damping ratio, or having uncharacteristically large damping (such as >10%). Put all modes that pass these thresholds into a new batch.

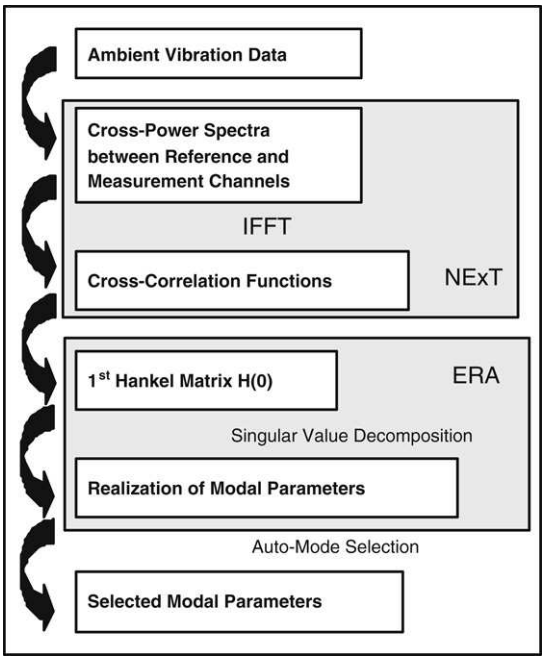


Fig. 10. Outline of procedure for system identification using NExT-ERA.

2. Compute the Modal Assurance Criterion (MAC). In this selection technique, the target mode obtained from a pool of realized modes are compared with their theoretical counterparts derived from a simple model of distributed mass system, whose jth mode is defined as

$$\Phi_j(x) = \sin(j\pi x). \tag{22}$$

The Modal Assurance Criterion (MAC) between a pair of modes is defined as:

$$MAC(\{\varphi^{an}\}_i, \{\psi^{id}\}_i) = \frac{|\{\varphi^{an}\}_i^t \{\psi^{id}\}_i^*|^2}{(\{\varphi^{an}\}_i^t \{\varphi^{an}\}_i^*)(\{\psi^{id}\}_i^t \{\psi^{id}\}_i^*)} \tag{23}$$

where the superscripts *an* and *id* denote the analytical and identified mode shape respectively. Only modes with MAC values higher than 80% are selected.

3. Next, if there are more than two similar modes that have MAC values higher than 80% and both having natural frequencies within 10% of each other, the modes are ranked according to their EMAC values. The mode that has the highest EMAC value is selected and considered as the real mode.

By employing the three procedures above, the real modes can automatically be retrieved from a pool of ERA-generated modes. The complete procedure of identification using NExT-ERA is illustrated in Fig. 10.

5.2. Trend of natural frequencies and damping ratios

During measurement, wind velocity varied from 3 to 15 m/s. As the result, the root-mean-square (*rms*) of the girder's vertical acceleration response also varied from 0 to 3 cm/s^2 as shown in Fig. 11. This allows us to observe the effects of wind velocity to the modal parameters. Fig. 12 shows the

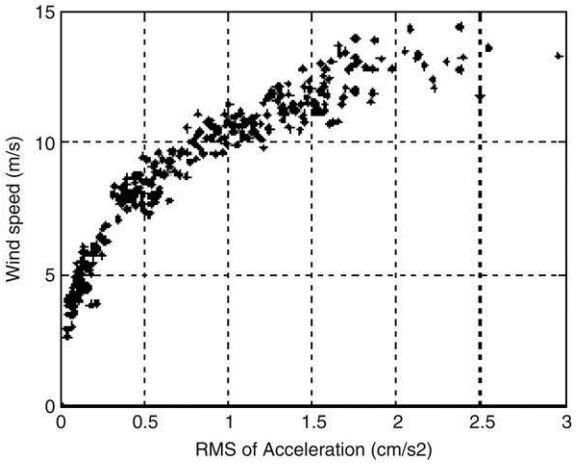


Fig. 11. Relationship between wind speed and RMS of girder vertical acceleration.

amplitude dependency of natural frequency and damping ratio with respect to *rms* of acceleration measured at channel Z17. Note that the acceleration in the horizontal axis of Fig. 12 is proportional to the wind speed as shown in Fig. 11. The natural frequencies of the first mode are within the range of 0.125–0.135 Hz, and vary about 4.6% from its mean value. Natural frequencies of the second mode are within the range of 0.150–0.157 Hz, with the variation of 2.2% from its mean value. Damping ratios are rather scattered within 0.2%–6% for the first mode and 0.1%–5% for the second mode. Variation of natural frequency and damping ratio are regarded as acceptable considering that measurement was conducted under various wind speeds. Despite the variations or dispersions of natural frequencies and damping ratios, there seem to be clear trends between frequencies, damping ratios and acceleration amplitude (consequently, the wind speed). In Fig. 12 one can notice that in general the natural frequencies decrease as the wind velocities increase. Although damping values are rather scattered, the overall identified damping ratios reveal an increasing trend as the wind velocities increase. The decrease and increase of natural frequencies and damping ratios are more apparent in the low-order modes as evident by the slopes of the linear trend.

The results of wind tunnel tests are also shown in the figures. Wind tunnel experiments conducted with a sectional model to obtain the aerodynamic damping and aerodynamic stiffness [27]. The wind tunnel results suggest that the natural frequency of vertical bending mode increases slightly as the wind speed increases due to aerodynamic effects. Furthermore, it is expected to increase significantly under stronger winds according to the prediction of the self-exciting aerodynamic force that was obtained in the wind tunnel experiment. The similarity of the aerodynamic damping effect on vertical modes is observed in both wind tunnel experiments and the identification results. The results on aerodynamic stiffness from wind tunnel tests, however, are different from identification results. This difference is due to the effect of the stiffness at the bearing near the towers, which was not included during wind tunnel tests [27]. The cause of discrepancies in natural

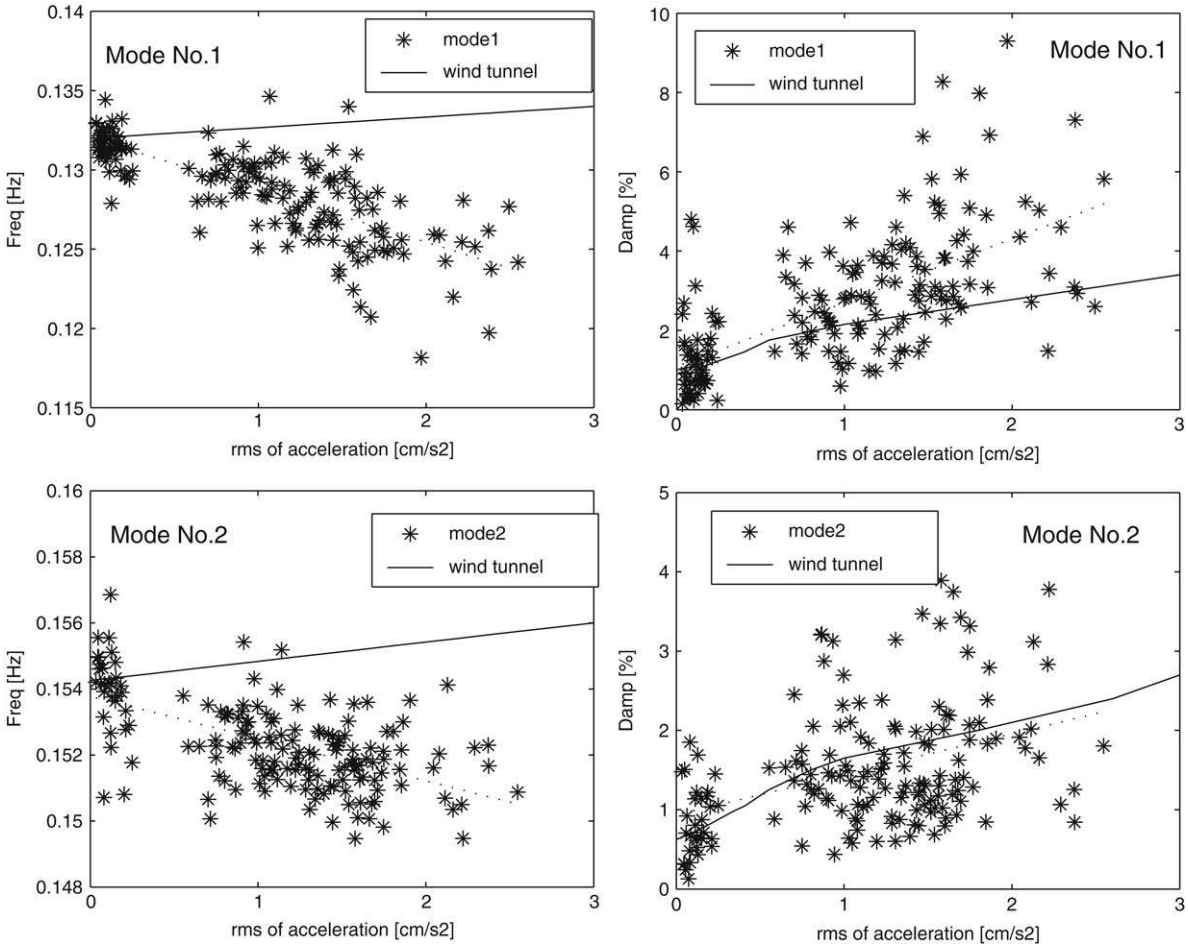


Fig. 12. Amplitude dependency of natural frequency and damping ratio for (a) 1st vertical bending mode (b) 2nd vertical bending mode and their comparison with wind tunnel test.

frequency and damping ratio appear to be the effect of stick–slip behavior of Coulomb friction elements in the bearing located near the towers. It seems that during lower wind velocity the bearings remain stuck thus causing higher stiffness. On the other hand, during higher wind velocity the bearings slide with certain friction forces and result in lower stiffness.

5.3. Mode shape and modal phase angle

The mode shape components reveal two different trends. The real parts of mode shape vectors do not exhibit a distinct trend, indicating no obvious changes of modes. The modal phase angle computed from the imaginary part of the mode shape vectors, however, revealed a clear trend. A phase difference exists between the closest measurement location to the main tower (Z6) and the measurement location at the center of the main span (Z17). It was observed that the phase difference is large when the acceleration *rms* is very small and decreases when the acceleration *rms* becomes large (Fig. 13).

These phase differences indicate that the system is non-proportionally damped. The locality effect of phase difference that was concentrated mainly at the edge of girder suggests the contribution of additional damping and stiffness caused by friction force at the bearings. In addition, the decrease and increase of natural frequencies and damping ratios indicated the effect of aerodynamic force along the girder. To study the extent of these effects, they were modeled as additional stiffness and damping: (1) located at the edge of girder to represent the friction force at bearings and expansion devices, and (2) distributed alongside the girder to illustrate the aerodynamic forces (Fig. 14).

In order to quantify the additional stiffness and damping an inverse analysis was performed. In the inverse analysis [22, 28], one set of modal parameters identified from 2-hour measurement was chosen as reference or ‘original’ (i.e. without additional stiffness and damping), whereas the other sets of identified modal parameters were regarded as the systems that consist of the additional stiffness damping alongside its girder and near the edge. In the subsequently related research [28], it was found that the contribution of aerodynamic force was much smaller than the effect of friction force at the bearing. The aerodynamic force contribution is in order of one-percent when compared to the contribution of the friction force, and its behavior is in agreement with the aerodynamic force obtained from wind tunnel results. Furthermore, the additional damping and stiffness due to friction force display clear trends.

Fig. 15 shows that when the *rms* acceleration is small, the damping is also small while the stiffness is large. This result

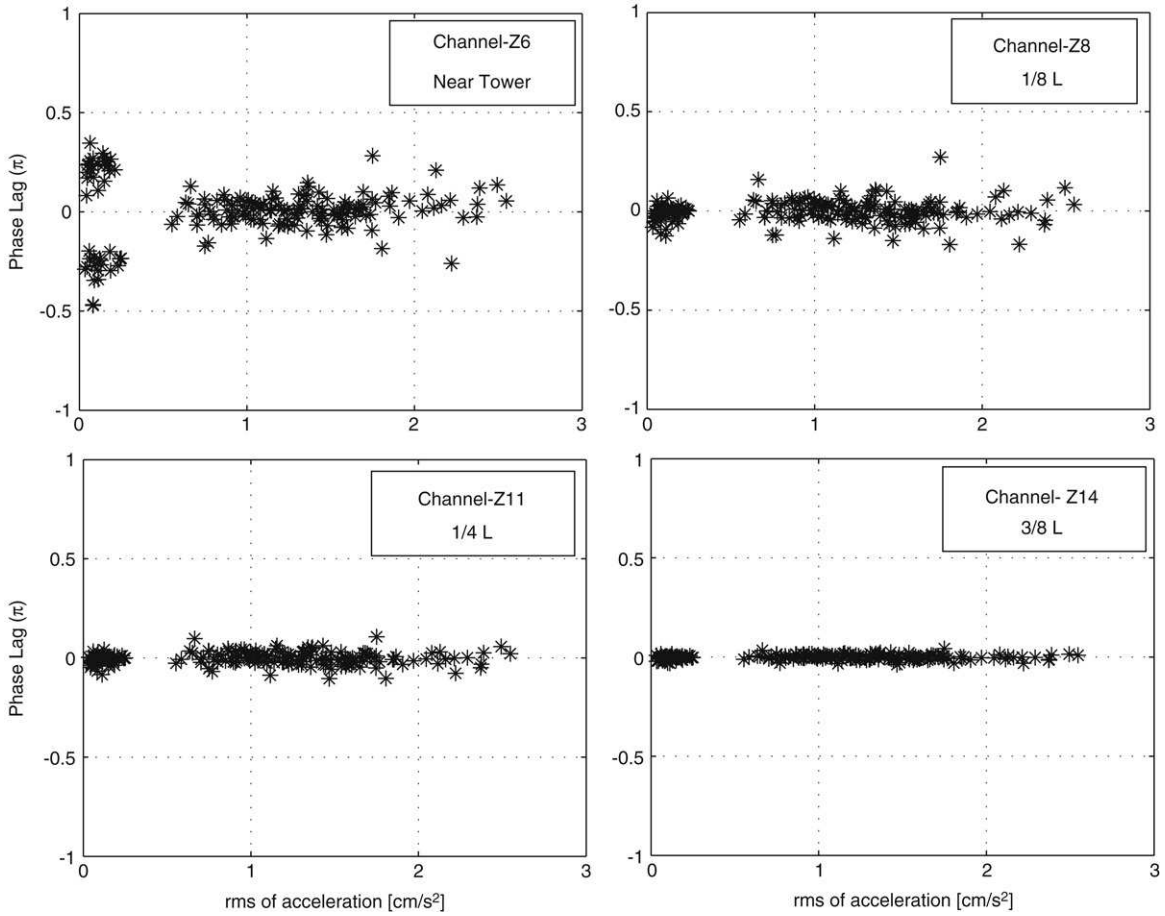


Fig. 13. Phase Lag of the first mode with respect to *rms* of vertical acceleration (Note: L = total length of the middle span).

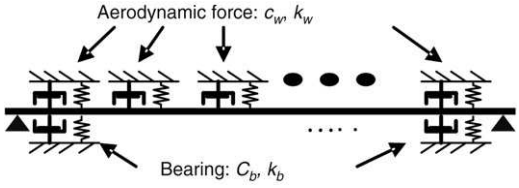


Fig. 14. Modeling of the bridge used in the identification of additional stiffness and damping at bearing and aerodynamic.

is consistent with the expected increase in equivalent stiffness as well as decrease in damping when the amplitude level is small enough to prevent any slip mechanism at the bearing or extension devices near the towers. When the wind speed increases the damping is also increases, which is when the bearings are unstuck, whereas the stiffness is decreasing as the result of increasing flexibility of the structure.

6. Concluding remarks

This study has presented a schematic data analysis and evaluation of system identification procedures to obtain dynamic characteristics of the Hakucho Suspension Bridge using ambient response. The free vibration responses of the bridge have been derived from ambient vibration responses using Random Decrement and Natural Excitation technique. Subsequently, two output-only system identification methods,

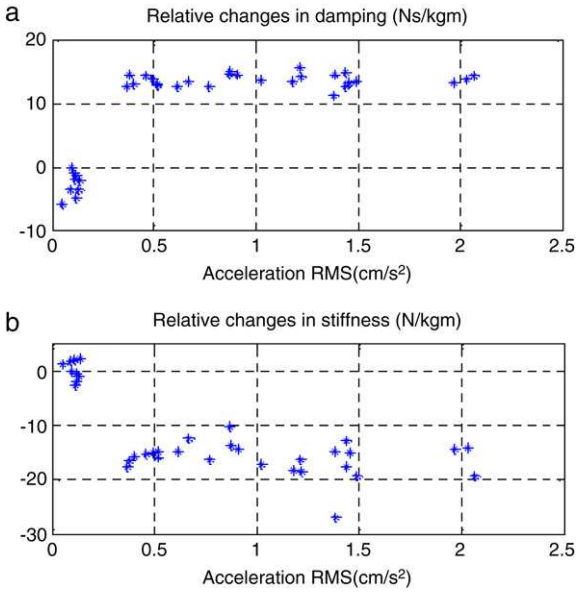


Fig. 15. (a) Equivalent changes in damping (b) Equivalent changes in stiffness due to friction force at bearing.

ITD and ERA, have been employed. The effectiveness and accuracy of both methods have been investigated. The following conclusions are drawn from the study:

1. Direct implementation of ITD method can only identify several low-order modes. The higher-frequency modes can be estimated by employing a successive filtering technique that follows the original ITD method. This method is shown to give an excellent result even for structure having closely spaced frequencies such as the Hakucho Suspension Bridge.
2. In implementation of ERA, a post-processing procedure was employed after realization of modal parameters. This procedure facilitates the selection of genuine modes from computational or fictitious modes that often characterize the ERA results. The method worked well by setting threshold values of EMAC, MAC and damping ratios of the acceptable identification results.
3. Although both ITD and ERA methods were found to be reliable in identifying modal parameters, the performance of the NExT-ERA technique was much better in regard to the efficiency in dealing with voluminous measurement data.
4. Owing to detailed measurement and dense sensor deployment, modal characteristics up to 24 modes can be identified from ambient vibration records. The identified natural frequencies and mode shapes were in good agreement with the results of FEM. There are still some issues on the scattering of damping ratios that need further investigation. Nevertheless, the overall results have demonstrated that reliable information about dynamic behaviors of the bridge can be obtained from a low cost, straightforward and non-invasive ambient vibration test.
5. Dynamic characteristics of the bridge exhibited dependencies of natural frequency, damping ratio and the modal phase angle on response amplitude level (i.e. wind velocity). The cause of these dependencies appear to be the effect of aerodynamic forces alongside the girder, and the friction force from bearings at the towers.

The importance of this work is placed on the application of efficient and reliable system identification in dealing with voluminous measurement data. These two important features could lead to a systematic approach in structural health monitoring and application of structural damage detection to a long span bridge using ambient vibration.

Acknowledgement and disclaimer

The authors wish to express their gratitude to the Hokkaido Regional Development Bureau, Ministry of Land, Infrastructure and Transport, Government of Japan for providing the ambient records and construction drawings of the bridge. The first author is grateful to the Japan Society of Promotion Science (JSPS), whose postdoctoral fellowship program supports his stay in Japan during the completion of this work. Opinions, findings and conclusions stated on this paper are of the authors and do not necessarily reflect those of the Hokkaido Development Bureau, Ministry of Land, Infrastructure and Transport.

References

[1] Abdel-Ghaffar AM, Housner GW. Ambient vibration tests of suspension bridge. Journal of Engineering Mechanics Division, ASCE 1978;104(5): 983–99.

[2] Abdel-Ghaffar AM, Scanlan RH. Ambient vibration studies of Golden Gate bridge, I: Suspended structure. Journal of Engineering Mechanics, ASCE 1985;111(4):463–82.

[3] Catbas FN, Aktan AE. Vibration testing of a long span bridge: Objectives and challenges. In: Proc. of the 17th IMAC, vol. I. 1999. p. 166–73.

[4] Brownjohn JMW, Dumanoglu AA, Severn RT, Taylor CA. Ambient vibration measurements of the Humber Suspension Bridge and comparison with calculated characteristics. Proceeding of the Institution of Civil Engineers Part 2 1987;83:561–600.

[5] Cunha A, Caetano E, Delgado R. Dynamic tests on large cable-stayed bridge. Journal of Bridge Engineering 2001;6(1):54–62.

[6] Peeters B, Maeck J, De Roeck G. Stochastic system identification for operational modal analysis: A review. Journal of Dynamic Systems, Measurement, and Control 2001;123(4):659–67.

[7] Ibrahim SR. Random decrement technique for modal identification of structures. The AIAA Journal of Spacecraft and Rockets 1977;14(11).

[8] Ibrahim SR, Mikulcik EC. A method for direct identification of vibration parameters from the free response. The Shock and Vibration Bulletin 1977;47(4):183–98.

[9] Farrar CR, James III GH. System identification from ambient vibration measurements on a bridge. Journal of Sound and Vibration 1997;205(1): 1–18.

[10] Juang JN, Pappa RS. An eigensystem realization algorithm for modal parameter identification and model reduction. Journal of Guidance, Control, and Dynamics 1985;8(5):620–7.

[11] Bendat JS, Pierson AG. Engineering applications of correlation and spectral analysis. New York: John Wiley; 1980.

[12] Brincker R, Zhang LM, Andersen P. Modal identification from output-only system using frequency domain decomposition. Smart Materials and Structures 2001;10:441–5.

[13] Maia NM, Silva JMM. Theoretical and experimental modal analysis. 2nd ed. Research Studies Press LTD and John Wiley & Sons INC; 1997.

[14] Deblauwe F, Brown DL, Allemang RJ. The polyreference time domain technique. In: Proc of the 5th IMAC, vol. 2. Union College; 1987. p. 832–45.

[15] Brown DL, Allemang RJ, Zimmerman R, Mergeay M. Parameter estimation techniques for modal analysis. SAE Paper. 1979.

[16] Van Overschee P, De Moor B. Subspace identification for linear systems: theory–implementation–applications. Dordrecht (The Netherlands): Kluwer Academic Publishers; 1996.

[17] Gersch W, Nielsen NN, Akaike H. Maximum likelihood estimation of structural parameters from random vibration data. Journal of Sound and Vibration 1973;31(3):295–308.

[18] Huang CS, Yang YB, Lu LY, Chen CH. Dynamic testing and system identification of a multi-span highway bridge. Earthquake Engineering & Structural Dynamics 1999;28(8):857–78.

[19] Chiang DY, Cheng MS. Modal parameter identification from ambient response. AIAA Journal 1999;37(4):513–5.

[20] Ibrahim SR, Pappa RS. Large modal survey testing using the Ibrahim Time Domain identification technique. Journal of Spacecraft and Rockets 1982;19(5):459–65.

[21] Tamura Y, Suganuma S. Evaluation of amplitude-dependent damping and natural frequency of buildings during strong winds. Journal of Wind Engineering & Industrial Aerodynamics 1996;59(2):115–30.

[22] Siringoringo DM, Fujino Y. Experimental study of laser Doppler vibrometer and ambient vibration for vibration-based damage detection. Engineering Structures 2006;28(13):1803–15.

[23] Caicedo JM, Dyke SJ, Johnson EA. Natural excitation technique and eigensystem realization algorithm for phase I of the IASC-ASCE benchmark problem: Simulated data. Journal of Engineering Mechanics (ASCE) 2004;130(1):49–60.

[24] Vandiver JK, Dunwoody AB, Campbell RB, Cook MF. A mathematical basis for the random decrement vibration signature analysis technique. Journal of Mechanical Design 1982;104:307–13.

[25] Ho BL, Kalman RE. Effective construction of linear state variable models for input output functions. Regelungstechnik 1966;14:545–8.
[26] Juang JN, Pappa RS. Effects of noise on modal parameter identification. Journal of Guidance 1986;295–303.
[27] Hokkaido Development Bureau: Report on wind tunnel experiments of girder of Hakucho Bridge. 1994 [in Japanese].
[28] Nagayama T, Abe M, Fujino Y, Ikeda K. Structural identification of a nonproportionally damped system and its application to a full-scale suspension bridge. Journal of Structural Engineering (ASCE) 2005; 131(10):1536–45.